Vol 18 No 5, May 2009
1674-1056/2009/18(05)/1923-08

Chinese Physics B

© 2009 Chin. Phys. Soc.
and IOP Publishing Ltd

Study of the theoretical tensile strength of Fe by a first-principles computational tensile test*

Liu Yue-Lin(刘悦林), Zhang Ying(张 颖),
Hong Rong-Jie(洪荣杰), and Lu Guang-Hong(吕广宏)†

Department of Physics, Beijing University of Aeronautics and Astronautics, Beijing 100191, *China*

(Received 6 June 2008; revised manuscript received 23 October 2008)

This paper employs a first-principles total-energy method to investigate the theoretical tensile strengths of bcc and fcc Fe systemically. It indicates that the theoretical tensile strengths are shown to be 12.4, 32.7, 27.5 GPa for bcc Fe, and 48.1, 34.6, 51.2 GPa for fcc Fe in the [001], [110] and [111] directions, respectively. For bcc Fe, the [001] direction is shown to be the weakest direction due to the occurrence of a phase transition from ferromagnetic bcc Fe to high spin ferromagnetic fcc Fe. For fcc Fe, the [110] direction is the weakest direction due to the formation of an instable saddle-point 'bct structure' in the tensile process. Furthermore, it demonstrates that a magnetic instability will occur under a tensile strain of 14%, characterized by the transition of ferromagnetic bcc Fe to paramagnetic fcc Fe. The results provide a good reference to understand the intrinsic mechanical properties of Fe as a potential structural material in the nuclear fusion Tokamak.

Keywords: Fe, theoretical tensile strength, phase transition, first-principles computational tensile test

PACC: 6155F, 7115A, 7115M

1. Introduction

The theoretical (ideal) strength of materials is the stress which is required to force deformation or fracture at the elastic instability.[1] The theoretical strength sets an upper bound on the attainable stress. The strength of a real crystal can be changed by existing cracks, dislocations, grain boundaries and other microstructural features, but its theoretical value can never be increased.[1,2] The theoretical tensile strength is that a material becomes unstable with respect to fracture by the spontaneous separation of atomic planes. The upper limit of the tensile strength is of obvious interest for strong solids in atomic models,[1,3−7] since theoretical strength is an intrinsic material property which is determined by the behaviour of valence electrons and ions.

By virtue of the development of density-functional theory (DFT)[8,9] combined with band-theoretical schemes and the rapid progress in modern computers, the first-principles method can be applied to study different properties of materials.[10,11] Recently, it has become possible to do a first-principles computational tensile test (FPCTT) to investigate stress as a function of strain and obtain the theoretical tensile strength by deforming crystals to failure.[12] In FPCTT, symmetry is generally an important factor to determine the stress–strain relation and the calculated theoretical strength. For single crystals, earlier studies on the theoretical tensile strength of W, Cu, Ir and NiAl have been made by Sob *et al.*[13−15] So far, the theoretical tensile strength of fcc (Cu, Al and Ni) and bcc (Mo, W, Nb, Fe) metals have been published.[2,5,16−18] On the other hand, the theoretical strength can also be extended to defective systems containing only one defect such as a point defect,[19] an interface or a grain boundary.[20−27] The theoretical tensile strengths of a clean Al grain boundary (GB) and an Al GB containing Na, Ca, S, and Ga have been calculated in order to explore impurity-induced intergranular embitterment.[22−26,28] Correspondingly, different temperature mechanical properties of materials have also been investigated successfully under tensile strain using the molecular dynamics method.[29−31]

Iron is one of the important magnetic transition metals which have many applications. Its ground state is ferromagnetic bcc Fe (α-Fe), and another hcp Fe is computationally shown to be a possible metastable

*Project supported by the National Natural Science Foundation of China (Grant No 50771008) and New Century Excellent Talents in University of China.

†Corresponding author. E-mail: LGH@buaa.edu.cn

paramagnetic phase.[32] At an elevated temperature, ferromagnetic α-Fe will transform to fcc Fe (γ-Fe) and another bcc Fe (i.e., δ-Fe). A first-principles study reveals that fcc Fe corresponds to three possible metastable magnetic ordering phases, including a paramagnetic phase, a low-spin ferromagnetic phase and a high-spin ferromagnetic phase, with lattice parameters ranging from 0.344 to 0.380 nm.[32]

Ferritic steels represent promising high-performance candidate structural materials in the fusion Tokamak. Such materials must not only withstand radiation damage, but also keep their intrinsic mechanical properties and structural strength, and hence firstly it is necessary to ensure detailed understanding of the mechanical properties of these candidate materials, even for a single crystal. Although many efforts have been made on α-Fe (bcc Fe) using a first-principles method,[17,33] the theoretical strength of some crystalline directions of bcc Fe such as $\langle 110 \rangle$ is still lacking. It is well known that austenitic steels have been successfully applied to nuclear fission materials due to their high ductility, low yield stress and relatively high ultimate tensile strength, but little has been done on the theoretical mechanical properties of γ-Fe (fcc Fe).

In this paper, we perform FPCTT to investigate the theoretical stress–strain relations and tensile strength of both bcc and fcc Fe. A comparison has been made with the experimental tensile strength in the [001] direction of bcc Fe. The results will not only provide a good reference to study the mechanical properties of ferritic steels as the candidate structural materials for fusion, but also serve as a first step to investigate the effect of He on the mechanical properties of Fe.

2. Computational methods

We employ a total-energy method based on DFT[34,35] with the generalized gradient approximation (GGA).[36] The wave functions are obtained by solving the Kohn–Sham equation using a plane wave basis. The plane-wave kinetic energy cutoff is 340 eV. For summation over the Brillouin zone, an uniform grid of k-points is chosen according to the Monkhorst–Pack scheme.[37] All of the calculations have been carried out by using the Vienna *ab-initio* simulation package (VASP).[38,39] The spin polarization has been taken into account for bcc Fe because of a typical magnetic transition metal, while not considered for fcc Fe due to paramagnetism of high temperature. The interaction between ions and electrons is described by the projector augmented wave (PAW) potential based on GGA. The energy relaxation iterates until the forces on all the atoms are less than 10^{-2} eV/nm.

The calculated equilibrium lattice constants are 0.284 nm for bcc Fe and 0.344 nm for fcc Fe. This is slightly lower than the experimental datum 0.364 nm for fcc Fe, while the lattice constant value of bcc Fe is consistent with the corresponding experimental value of 0.287 nm. This demonstrates the accuracy of the current PAW method. In the FPCTT, an uniaxial tensile strain has been applied to the chosen crystalline directions. For the uniaxial tensile strain, the tensile stress $\sigma_{\alpha,\beta}$ $(\alpha, \beta = 1, 2, 3)$ is calculated from

$$\sigma_{\alpha,\beta} = \frac{1}{\Omega(\varepsilon)} \frac{\partial E}{\partial \varepsilon}, \tag{1}$$

where E is the total energy and $\Omega(\varepsilon)$ is the volume at the given tensile strain of ε.

The lattice vectors were incrementally added in the direction of the imposed strain. At each strain step, the structure was fully relaxed until all other five stress components vanished except that in the tensile direction. The tensile stress for each strain step can be calculated, and thus the stress–strain relationship and the theoretical tensile strength can be obtained.

3. Results and discussion

3.1. Theoretical tensile strength of bcc Fe

In the FPCTT of bcc Fe, we choose three representative directions including [001], [110] and [111]. Three unitcells with different symmetry are employed for the FPCTT in these three directions, as shown in Fig.1.

We first investigate the stress–strain relations of the [110] and [111] directions in bcc Fe. For the FPCTT in the two directions, the original unitcell exhibits an orthogonal structure as shown in Figs.1(b) and 1(c). Such symmetry will not change in the tensile process in the [110] and [111] directions. Figure 2(a) shows the strain energy as a function of strain. The strain energy increases with increasing strain, exhibiting an inflexion at the strain of 32% in the [110] direction and 30% in the [111] direction, respectively.

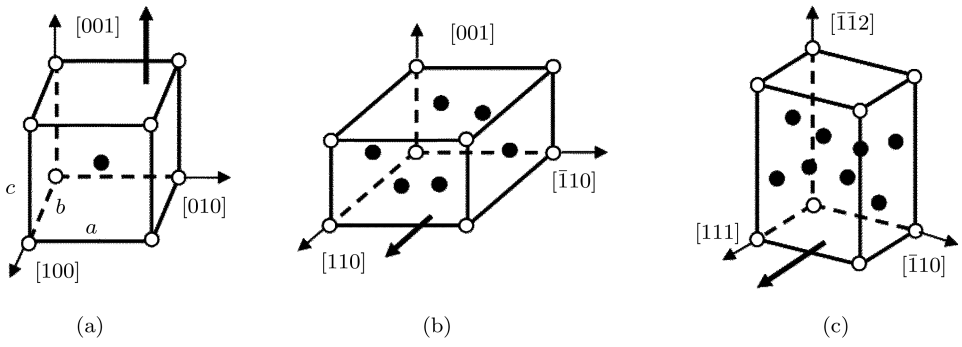


Fig.1. The geometric structure of unitcells of the bcc Fe in the [001], [110] and [111] directions used for FPCTT. (a) A bcc unitcell with 2 atoms inside for FPCTT in the [001] direction. (b) A general face-centred tetrahedral (fct) unitcell of Fe with 4 atoms inside for FPCTT in the [110] direction. (c) An orthorhombic unitcell with 6 atoms inside for FPCTT in the [111] direction. The thick arrows represent the respective tensile directions.

Correspondingly, as shown in Fig.2(b), the stresses increase with increasing strain until they reach a maximum of 32.7 GPa at a strain of 32% in the [110] direction and 27.5 GPa at a strain of 30% in the [111] direction, beyond which the stresses decrease. Thus, the theoretical tensile strengths are 32.7 GPa in the [110] direction and 27.5 GPa in the [111] direction, respectively.

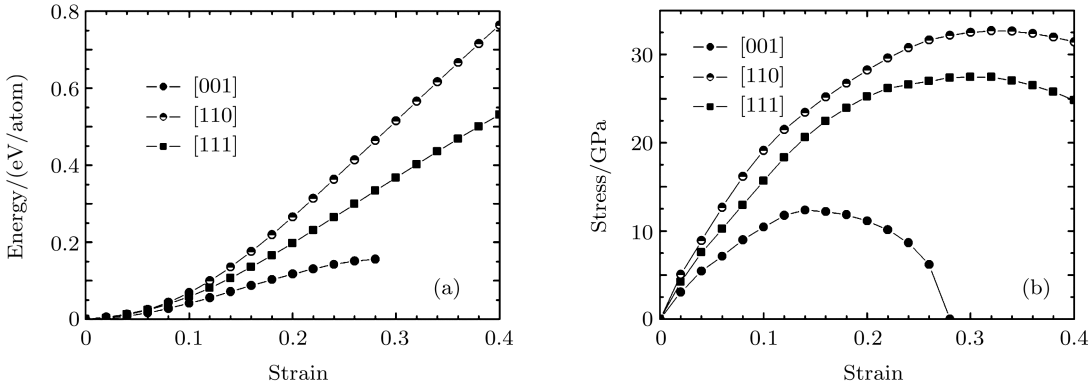


Fig.2. Energy (a) and stress (b) as a function of tensile strain in the [001], [110], and [111] directions in bcc Fe, respectively.

For the [001] direction, the stress increases with increasing strain, and exhibits a maximum of 12.4 GPa at a strain of 14%, corresponding to the inflexion in the strain energy-strain curve (Fig.2). Evolution of the cell geometry illustrated in Fig.3 is the well-known 'Bain Path', also investigated in the previous studies.[2,17] The initial zero-stress point corresponds to the initial bcc structure, in which the ratio of $a : b : c$ is $1 : 1 : 1$ (Fig.3(a)). With the increase of strain, the lattice parameters of a and b decrease, while c increases. When the

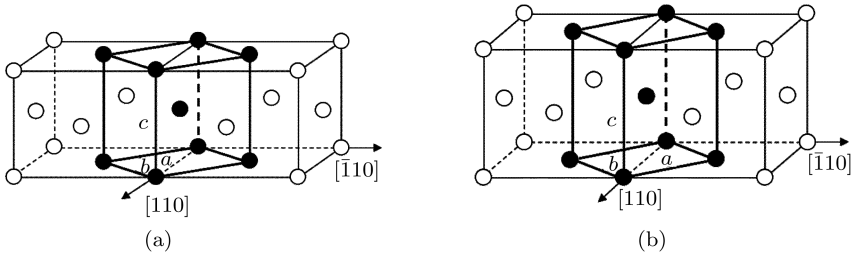


Fig.3. The evolution of the geometric structure of the unitcell of bcc Fe under tension in the [001] direction.

ratio of $a : b : c$ becomes $1 : 1 : \sqrt{2}$ (the strain of 28%), the stress reaches the second zero-stress point, leading to formation of a new fcc structure (Fig.3(b)). This structure corresponds to the saddle-point of the energy maximum in the energy–strain curve (Fig.2(a)). However, it is interesting to find that such an fcc structure is not an unstable structure but a metastable phase with a stress-free characteristic. Such a phase is the high spin ferromagnetism state of fcc Fe with a lattice constant of 0.363 nm, as computationally shown in the previous study.[32]

3.2. Magnetic instability and phase transition

Different from the [110] and [111] directions, the stress–strain relation in the [001] direction will become abnormal with the magnetic moment unconstrained in the tensile process. Both the energy–strain and stress–strain curves for the [001] direction differ obviously from those with the magnetic moment constrained as shown in Fig.4. Initially, the strain energy and stress

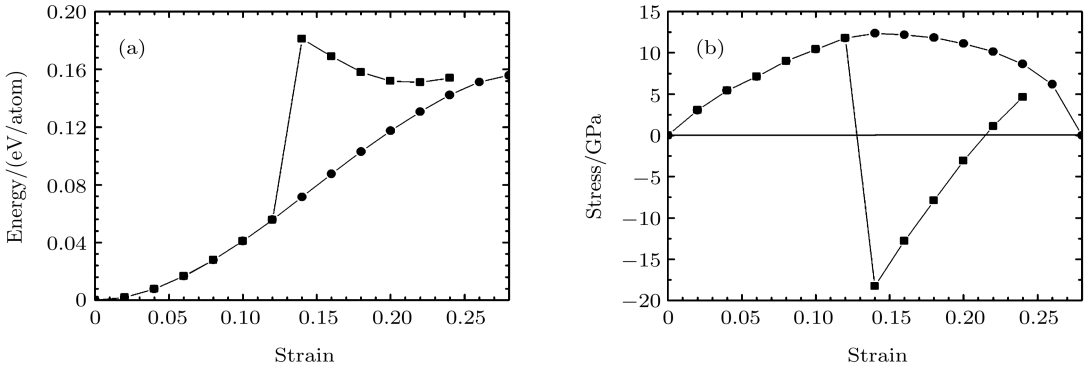
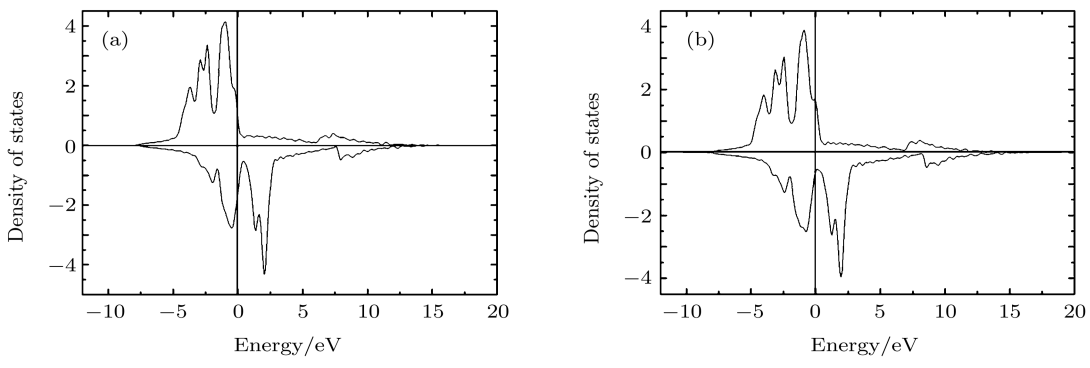


Fig.4. Energy (a) and stress (b) as a function of tensile strain in the [001] direction in bcc Fe. The circles represent the case that the magnetic moment is constrained, while the squares represent the case when the magnetic moment is not constrained.

increase with the increasing strain, the same as those with constrained magnetic moment. However, at the strain of 14%, the strain energy increases abruptly, and decreases again with further increase of strain. Correspondingly, stress exhibits a sudden drop to an abnormal negative value (Fig.4(b)).

Density of state (DOS) results for different strains point out the change of magnetic property of bcc Fe in the tensile process with the unconstrained magnetic moment as shown in Fig.5. The DOS of spin-up and spin-down remains asymmetric up to the strain of ∼14%, implying that bcc Fe is ferromagnetic. This corresponds to the smooth energy–strain and stress–strain curves before 14%. But, beyond the strain of 14%, DOS of spin-up and spin-down exhibits a symmetric characteristic. Such an abnormal transformation indicates an occurrence of a magnetic instability. However, such magnetic instability corresponds to a phase transition from ferromagnetism to paramagnetism (Fig.5(d)). The strain of 14% corresponds



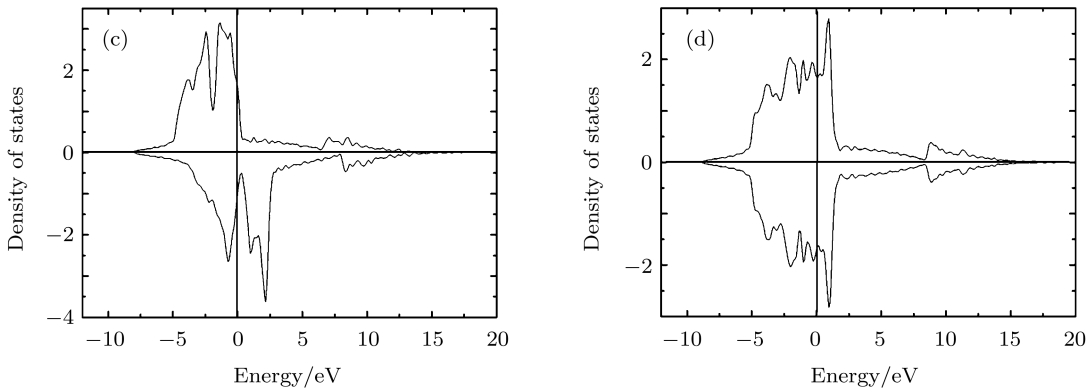


Fig.5. Density of states of bcc Fe at different strains: (a) 0%, (b) 6%, (c) 12% and (d) 14%. The Fermi energy for the respective case is set to be zero. A positive value represents spin-up and a negative value represents spin-down.

to the lattice parameter of 0.324 nm, smaller than 0.344 nm of the calculated equilibrium paramagnetic fcc Fe. Consequently, the stress becomes compressive (negative) starting from this strain. Further increase of strain leads to an energy minimum, as shown in Fig.4(a), at a strain of 22%, corresponding to another stress-free structure (Fig.4(b)). The lattice parameter of such a stress-free structure is exactly the same as that of equilibrium paramagnetic fcc Fe (0.344 nm), which indicates the occurrence of the phase transition from the ferromagnetic bcc Fe to the metastable paramagnetic fcc Fe. Such a metastable paramagnetic fcc Fe phase has been investigated by Kong and Liu recently.[32]

3.3. Theoretical tensile strength of fcc Fe

In the FPCTT of fcc Fe, we also choose three representative directions including [001], [110] and [111]. Three unitcells with different symmetry are employed for the FPCTT in different directions, as shown in Fig.6.

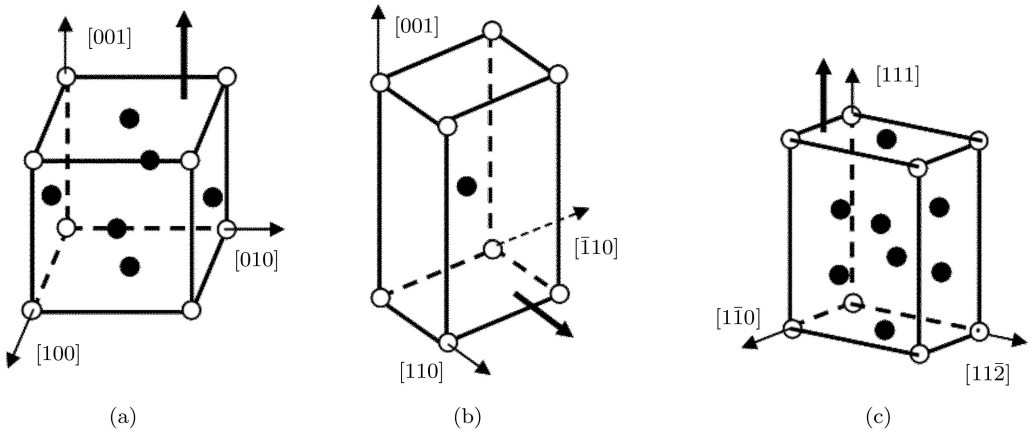


Fig.6. The geometric structure of tensile unitcells of fcc Fe in the directions [001], [110] and [111]. (a) A general fcc unitcell of Fe with 4 atoms. (b) A bct unitcell with 2 atoms. (c) A unitcell with 6 atoms.

For the FPCTT in the [001] direction, here we used the fcc unitcell which is drawn from the fcc crystal as shown in Fig.6(a). The original unitcell exhibits tetragonal symmetry. Such symmetry will not change in the tensile process in the [001] direction. Figure 7(a) shows the strain energy as a function of tensile strain. The strain energy increases with increasing strain, exhibiting an inflexion at the strain of 28%. Correspondingly, as shown in Fig.7(b), the stress increases with increasing strain until it reaches a maximum of 48.1 GPa at a strain of 28%, beyond which the stress decreases. Thus, the theoretical tensile strength is 48.1 GPa in the [001] direction.

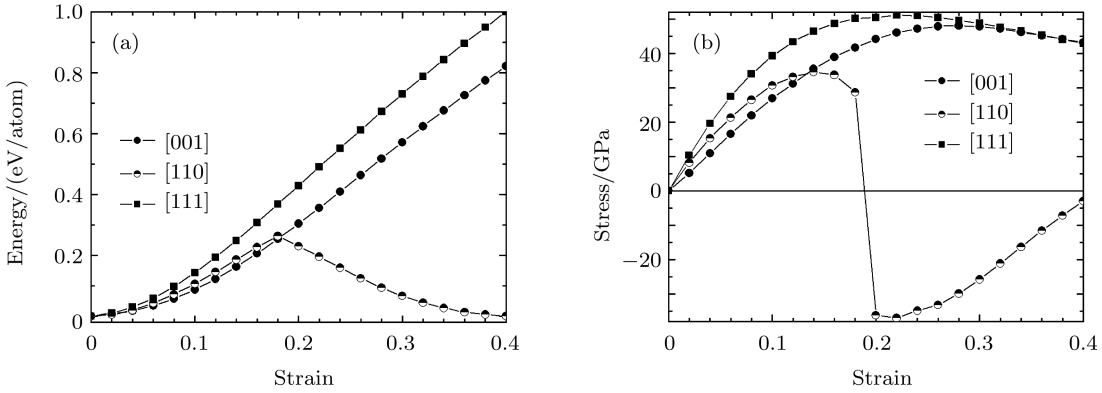


Fig.7. Energy (a) and stress (b) as a function of tensile strain in the [001], [110] and [111] directions in fcc Fe, respectively.

Next, we perform the FPCTT in the [111] direction, the unitcell of which is shown in Fig.6(c). Similar to the [001] direction, Fig.7(b) shows that the stress reaches a maximum of 51.2 GPa at a strain of 22%, corresponding to the inflexion in the energy–strain curve (Fig.7(a)). The theoretical tensile strength is thus 51.2 GPa in the [111] direction.

As we can see from Fig.7(b), the stress–strain relation in the [110] direction differs from the [001] and [111] directions obviously. The unitcell we used for this direction is the bct shown in Fig.6(b). The strain energy as a function of strain is shown in Fig.7(a). The energy increases first with increasing strain, then reaches a maximum at a strain of 18%, after which the energy decreases to zero again at a strain of 40%. The maximum or minimum of the strain energy corresponds to zero stress points in the stress–strain curve in [110]. As shown in Fig.7(b), the stress exhibits one maximum of 34.6 GPa at a strain of 14%, then it goes back to the original structure again at a strain of 42%.

The zero-stress point in the stress–strain curve corresponds to a stress-free phase generated in the tensile process. The initial zero-stress point corresponds to the initial bct phase (fcc structure), as shown in Fig.8(a). The ratio of $a : b : c$ for such a phase is $1 : 1 : \sqrt{2}$. With the increase of strain, the lattice parameter of a increases, while c decreases and b remains almost unchanged, as shown in Fig.8. The lattice parameter of c is equivalent to a at a strain of 18%, where the stress reaches the second zero-stress point. At this point, there forms a new bct structure with $a = c > b$ (Fig.8(b)), different from the original one.

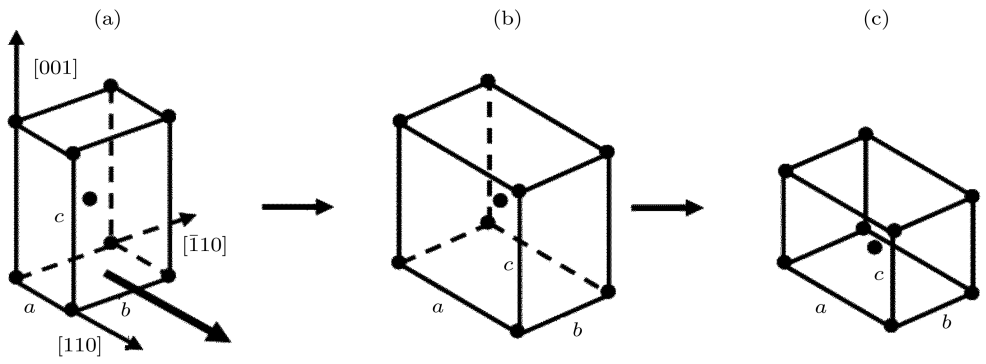


Fig.8. The evolution of geometric structures of the unitcell of fcc Fe under tension in the [110] direction.

This point corresponds to the saddle-point of the energy maximum (Fig.7(a)), which indicates that the new bct structure is an instable 'phase' despite its stress-free characteristic. Such a structure will evolve to other stable phases even with a small perturbation. With further increase of strain, the lattice parameter of c decreases continuously, and becomes equal to b at a strain of ∼20%. The ratio of $b : c : a$ becomes $1 : 1 : \sqrt{2}$ at the strain of 42% (Fig.8(c)), corresponding to the third stress-free point in the stress–strain curve. The present stress-free bct structure (i.e., fcc structure) is actually the same as the initial one (Fig.8(a)), but with a rotation of 90°. Consequently, the stress–strain relation after the strain of 42% should be exactly the same as that in the [001] direction shown in Fig.7(b).

The evolution of the cell geometry shown in Fig.9 is similar to the 'orthorhombic path', as investigated in previous studies.[2,17] It should be noted that the tensile process between the strains of 18% and 42% with the negative stress for the [110] direction is a virtual process and actually cannot occur. In the real process, the bct structure in the strain of 18% (Fig.8(b)) will evolve automatically to the final bct structure in the strain of 42% (Fig.8(c)).

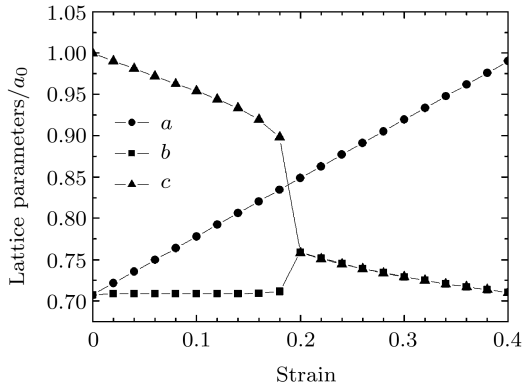


Fig.9. The lattice parameter in units of a_0 as a function of tensile strain in the [110] direction.

3.4. Comparison of the tensile strength of bcc and fcc Fe

We have respectively calculated the theoretical tensile strengths in the [001], [110] and [111] directions for bcc and fcc Fe as summarized in Table 1. For bcc Fe, the theoretical tensile strength in the [001] direction is 12.4 GPa according to the present calculation. This agrees well with 12.7 GPa and 12.6 GPa estimated by Sob *et al* [33] and Clatterbuck *et al*,[17] respectively.

Table 1. Theoretical tensile strengths in different crystalline directions for bcc and fcc Fe.

tensile direction	bcc Fe (GPa)	fcc Fe (GPa)
[001]	12.4[a]	48.1[a]
	12.7[b]	
	12.6[c]	
	30[d]	
[110]	32.7[a]	34.6[a]
[111]	27.5[a]	51.2[a]
	27.3[b]	
	46[d]	

[a]The present calculation.
[b]Calculation from Ref.[33].
[c]Calculation from Ref.[17].
[d]Calculation from Ref.[1].

The simplest calculation of a sinusoidal stress–strain relation originates from Polannyi and Orowan by using Eqs.(2) and (3) defined as

$$\sigma_{\max} = \sqrt{E\gamma/a_0}, \tag{2}$$

$$\varepsilon_{\max} = \frac{\pi}{2}\frac{\sigma_{\max}}{E}, \tag{3}$$

where a_0 is the equilibrium lattice constant, γ is the surface energy per unit area, and E is the Young's modulus. The calculated theoretical tensile strengths $\sigma_{\max}$ are 30 GPa in the [001] direction and 46 GPa in the [111] direction, and the associated maximum strains are 36% and 28%, respectively.[1]

On the other hand, in the present calculation, $\sigma_{\max}$ are 12.4 GPa at the strain of 14% in the [001] direction and 27.5 GPa at 30% in the [111] direction, respectively. It can be seen that there are large differences of the maximum stress and strain. One of the reasons for the differences lie in the fact that Eqs.(2) and (3) are only rough estimations. The calculated values depend strongly on the experimental values of surface energy γ and Young's modulus E, and the stress–strain relation is approximated to be sinusoidal.

Furthermore, in the present calculations, for bcc Fe, the [001] direction is the weakest with a theoretical tensile strength of ∼12.4 GPa, while the [110] and [111] directions are stronger. For fcc Fe, however, both [001] and [111] can be considered as stronger directions with theoretical tensile strength as large as ∼48 GPa and ∼51 GPa, respectively, while [110] is obviously a weak direction with a tensile strength of ∼34.6 GPa.

This can be understood on the basis of the following considerations. For bcc Fe, the (110) is the most-closely-packed crystalline plane, leading to the stronger interaction of atoms between the (110) planes

in comparison with the (001) and (111) planes. This makes the theoretical strength in the [110] direction higher than that in the [001] and [111] directions. However, although the (001) plane is more closely-packed in comparison with (111), the phase transition occurs in the [001] direction in the tensile process, making its tensile strength the lowest among the three directions. A similar analysis can be applied to the fcc Fe. The (111) is the most-closely-packed crystalline plane, thus it exhibits the highest theoretical tensile strength.

From Table 1, it can also be seen that the respective theoretical tensile strength in fcc Fe is larger than that in bcc Fe in the [001], [110] and [111] three tensile directions. This indicates the much higher ultimate tensile strength of fcc Fe than bcc Fe.

4. Conclusions

We have performed FPCTT based on the first-principles total-energy method to investigate the theoretical tensile strengths of bcc and fcc Fe systemically for understanding of the intrinsic mechanical properties of Fe. The theoretical tensile strengths are shown to be 12.4, 32.7 and 27.5 GPa for bcc Fe, and 48.1, 34.6 and 51.2 GPa for fcc Fe in the [100], [110] and [111] directions, respectively. For bcc Fe, the [001] direction is shown to be the weakest direction due to the occurrence of a phase transition from ferromagnetic bcc Fe to high-spin ferromagnetic fcc Fe with the lattice parameter of 0.363 nm. As for fcc Fe, the [110] direction is the weakest direction due to the formation of an unstable saddle-point 'bct structure' in the tensile process. Further, the DOS in the [001] direction for bcc Fe indicates the existence of a magnetic instability in the tensile process. Under tensile strains larger than 14% in the [001] direction, the ferromagnetic phase of bcc Fe becomes unstable and transforms to paramagnetic fcc Fe with the lattice parameter of 0.344 nm. These results will provide a good reference for Fe as a potential structural material in the nuclear fusion Tokamak.

References

[1] Kelly A and Macmillan N H 1986 *Strong Solids* 3rd ed. (Oxford: Clarendon Press)
[2] Luo W, Roundy D, Cohen M L and Morris Jr J W 2002 *Phys. Rev.* B **66** 094110
[3] Polanyi M 1921 *Z. Phys.* **7** 323
[4] Frenkel J 1926 *Z. Phys.* **37** 572
[5] Roundy D, Krenn C R, Cohen M L and Morris Jr J W 1999 *Phys. Rev. Lett.* **82** 2713
[6] Frenkel J 1926 *Z. Phys* **7** 323
[7] Orowon E 1949 *Rept. Prog. Phys.* **12** 185
[8] Hohenberg G P and Kohn W 1964 *Phys. Rev.* **136** B864
[9] Kohn W and Sham L J 1965 *Phys. Rev.* **140** A1133
[10] Hu Z H, He W, Sun Y and Cheng Z H 2007 *Chin. Phys.* **16** 3863
[11] Tian X Q, Du S X and Gao H J 2008 *Chin. Phys.* B **17** 0286
[12] Morris Jr J W and Krenn C R 2000 *Philos. Mag.* A **80** 2827
[13] Sandera P, Pokluda J, Wang L G and Sob M 1997 *Mater. Sci. Eng.* A **234–236** 370
[14] Sob M, Wang L G and Vitek V 1997 *Mater. Sci. Com.* A **234–236** 1075
[15] Sob M, Wang L G and Vitek V 1998 *Philos. Mag.* B **78** 653
[16] Ogata S, Li J and Yip S 2002 *Science* **298** 807
[17] Clatterbuck D M, Chrzan D C and Morris Jr J W 2003 *Acta. Mater.* **51** 2271
[18] Liu Y L, Zhang Y, Zhou H B, Lu G H and Kohyama M 2008 *J. Phys.: Condens. Matter* **20** 335216
[19] Deyirmenjian V B, Heine V, Payne M C, Milman V, Lynden-Bell R M and Finnis M W 1995 *Phys. Rev.* B **52** 15191
[20] Kohyama M 1999 *Philos. Mag. Lett.* **79** 659
[21] Kohyama M 2002 *Phys. Rev.* B **65** 184107
[22] Lu G H, Deng S H, Wang T M, Kohyama M and Yamamoto R 2004 *Phys. Rev.* B **69** 134106
[23] Lu G H, Zhang Y, Deng S, Wang T, Kohyama M, Yamamoto R, Liu F, Horikawa K and Kanno M 2006 *Phys. Rev.* B **73** 224115
[24] Zhang Y, Lu G H, Wang T, Deng S, Kohyama M and Yamamoto R 2006 *Mater. Trans.* **47** 2678
[25] Zhang Y, Lu G H, Hui X L, Wang T, Kohyama M and Yamamoto R 2007 *J. Phys.: Condens. Matter* **19** 456225
[26] Zhang Y, Lu G H, Deng S, Wang T, Xu H, Kohyama M and Yamamoto R 2007 *Phys. Rev.* B **75** 174101
[27] Liu L H, Zhang Y, Lu G H, Deng S H and Wang T M 2008 *Acta Phys. Sin.* **57** 4428 (in Chinese)
[28] Zhang Y, Lu G H, Deng S H and Wang T M 2006 *Acta Phys. Sin.* **55** 2901 (in Chinese)
[29] Wang Z G, Zu X T, Gao F and Weber W J 2006 *Appl. Phys. Lett.* **89** 243123
[30] Wang Z G, Zu X T, Gao F and Weber W J 2007 *Appl. Phys. Lett.* **90** 161923
[31] Lai W S and Zhao X S 2004 *Appl. Phys. Lett.* **85** 4340
[32] Kong L T and Liu B X 2004 *Appl. Phys. Lett.* **84** 3627
[33] Friak M, Sob M and Vitek V 2003 *Philos. Mag.* **83** 3529
[34] Hohenberg G P and Kohn W 1964 *Phys. Rev.* **136** B 864
[35] Kohn W and Sham L J 1965 *Phys. Rev.* **140** A 1133
[36] Perdew J P and Wang Y 1992 *Phys. Rev.* B **45** 13244
[37] Monkhorst H J and Pack J D 1976 *Phys. Rev.* B **13** 5188
[38] Kresse G and Hafner J 1993 *Phys. Rev.* B **47** 558
[39] Kresse G and Furthmüller J 1996 *Phys. Rev.* B **54** 11169